3422 *Macromolecules* **2010**, *43*, 3422–3428
DOI: 10.1021/ma1001589

Macromolecules
ARTICLE

Vibrational Eigenfrequencies and Mechanical Properties of Mesoscopic Copolymer Latex Particles

Tim Still,*,† Markus Retsch,†,∥ Ulrich Jonas,‡,† Rebecca Sainidou,§ Pascal Rembert,§ Konstantinos Mpoukouvalas,† and George Fytas‡,†

†*Max Planck Institute for Polymer Research, Ackermannweg 10, 55128 Mainz, Germany,* ‡*Department of Materials Science and Technology, University of Crete and FORTH, 71110 Heraklion, Greece, and* §*Laboratoire Ondes et Milieux Complexes LOMC FRE CNRS 3102, Université du Havre, Pl. R. Schuman, 76610 Le Havre, France.* ∥*Present address: Massachusetts Institute of Technology, 77 Massachusetts Avenue, Cambridge, MA.*

Received January 21, 2010; Revised Manuscript Received March 6, 2010

ABSTRACT: We report on the thermally excited resonance vibrations of mesoscopic poly(methyl-methacrylate)-poly(*n*-butylacrylate) (PMMA-P*n*BA) random copolymer colloidal spheres with varying *n*BA volume fractions. All systems but the bulk P*n*BA are in the glassy state at room temperature. Brillouin light scattering (BLS), dielectric spectroscopy (DS), and standard polymer characterization techniques reveal the homogeneity of this copolymer system down to the segmental length scale. Theoretical density-of-states calculations allow the determination of the shear modulus of the copolymer latex spheres from their eigenvibration BLS spectra. The representation of the copolymer longitudinal modulus by Wood's law, combining the PMMA and P*n*BA homopolymers values, succeeds if a higher fictive "glassy P*n*BA" modulus instead of the actual modulus of the neat P*n*BA rubber at room temperature is assumed. This is justified by the dynamic homogeneity of these copolymers exhibiting a single α-relaxation. A facile tuning of the thermomechanical properties of latex spheres via the copolymer composition as well as their experimental determination at a single sphere level becomes feasible.

Introduction

Copolymers are single polymeric entities composed of two or more monomeric species and present interesting material properties because they combine the features of the constituting monomers. Such material properties, like the glass-transition temperature, crystallinity, solubility, and toughness, can be modulated in a wide range by polymer synthesis with the type and ratio of the incorporated comonomers. For example, the combination of monomers from homopolymers of substantially different glass-transition temperatures can lead to a copolymer with an intermediate glass-transition temperature that can be tuned by the monomer ratio in the copolymer. As such, copolymers find a vast range of technical and commercial applications in various formats, from the bulk over thin films and coatings to latex particles.

In particular, copolymer latex particles have entered our every day life, for example, in paints and glue. As these latex particles usually have dimensions below the micrometer range, the exact determination of their mechanical properties is difficult but of high relevance for such technical applications. On this microscopic scale, the copolymeric materials may show homogeneous properties, like a single glass transition, whereas on the nanoscopic level of single chain segments, the local dynamics might be heterogeneous.[1] Also, from a fundamental point of view, the nondestructive access to the elastic properties and the glass transition(s) on the submicrometer scale is a challenging task, whereas the validity of an effective medium model on this length scale will allow a reliable prediction of the composition dependence of the thermomechanical properties. The applicability of an effective medium model is not trivial because at the local segmental level, the system can be heterogeneous. The dynamic heterogeneity, which is expressed by the presence of two well-separated segmental relaxation times, seems to be the rule in thermodynamically miscible polymer blends[2,3] and block copolymers exhibiting a single glass transition.[4−6]

To address the aforementioned tasks, we have selected the random copolymer poly(methyl methacrylate)-*r*-poly(*n*-butyl acrylate) (PMMA-*r*-P*n*BA) on the account of very similar reactivity, very different glass-transition temperature, T_g, of the corresponding homopolymers PMMA (T_g = 386 K) and P*n*BA (T_g = 230 K), and the different dynamic state of the PMMA (glassy) and P*n*BA (rubber) under ambient conditions. We employ Brillouin light scattering (BLS) to measure the particle vibration frequencies in multiply scattering colloidal crystals from which, in combination with different polymer characterization techniques, the longitudinal and shear moduli are determined using single-sphere scattering and density-of-states (DOS) computations for individual copolymer spherical particles. Both longitudinal ($M = \rho c_l^2$) and shear ($G = \rho c_t^2$) moduli as well as the Young's modulus ($E = \rho c_l^2(1 + \sigma)(1 - 2\sigma)/(1 - \sigma)$), with longitudinal and transverse sound velocities, c_l and c_t, respectively, and Poisson's ratio, σ, were found to decrease with increasing volume fraction (ϕ) of the softer P*n*BA component (i.e., lower T_g and moduli), resembling the trend of $T_g(\phi)$. $M(\phi)$ conforms to Wood's effective medium expression,[7,8] using for PMMA the corresponding bulk modulus value M_{PMMA}, but for the P*n*BA component, a much higher (∼40%) value than its experimental M_{PnBA} at ambient temperature. This unsuspected environment effect is supported by the homogeneous local dynamics in pressed films of the copolymers, which exhibit a

*To whom correspondence should be addressed. E-mail: still@mpip-mainz.mpg.de.

 Published on Web 03/12/2010

single α-relaxation, probed by dielectric spectroscopy (DS). Therefore, MMA and *n*BA segments are locally mixed down to the length scale of the Kuhn segment, and *n*BA units exist in the glassy and not the rubbery state of the bulk P*n*BA at ambient temperature.

The physical basis of the BLS is the inelastic scattering of light by phonons in the hypersonic (GHz) frequency range, utilizing high-resolution multipass tandem Fabry−Pérot interferometers. In BLS spectroscopy of transparent samples, the desired dispersion relation is obtained by recording the phonon frequencies as a function of the scattering wavevector, **q**, with magnitude $q = (4\pi/\lambda)\sin(\theta/2)$ (λ is the wavelenth of the laser in the material, and θ is the scattering angle). For samples, however, which exhibit strong multiple light scattering, as for the dry colloidal crystals or dry powders of the particles, **q** is ill-defined, and hence **q**-dependent acoustic-like modes become inaccessible for spontaneous BLS (however, access by two-laser methods remains possible[9]). Although, localized in space, that is, **q**-independent modes can be recorded in the BLS spectrum. These **q**-independent frequencies have been identified as the resonance modes of the individual colloidal particles, uniquely defined by the geometrical and elastic characteristics of the particles. BLS can record numerous thermally excited elastic resonances in one measurement.[10−14] Many fewer eigenmodes can be observed by Raman scattering for much smaller particles.[15,16] The number of resolvable modes is limited by selection rules that play only a role for particles with diameter much smaller than the wavelength of the probing light.[16−18] By the competitive pump−probe technique, only a few artificially excited resonance modes can be observed in mesoscopic[19] and nanoscopic[20] systems. Herein, we use a combined approach of **q**-dependent BLS, **q**-independent BLS, and additional characterization techniques to follow systematically the elastic moduli (M, G) of the individual particle, that is, its longitudinal and transverse sound velocities, c_l and c_t, respectively.

The article is organized as follows: The synthesis and characterization of the copolymer colloids and the BLS and DS experimental techniques are presented in the Experimental Section. In the next section, the identification of the obtained resonances in the BLS spectra is realized by appropriately adjusting the corresponding single-sphere eigenmodes and utilizing additional information obtained by angle-dependent BLS. The analysis of the segmental dynamics manifested in the DS spectra of the copolymer films is presented in the same section. In the succeeding Discussion, the physical meaning of the parameters in the effective medium model of the $M(\phi)$ along with the sensitivity of low eigenfrequencies to the shear modulus is rationalized.

Experimental Section

Samples. *Materials*. Methyl methacrylate (99%, Aldrich, MMA) and *n*-butyl acrylate (99%, Aldrich, *n*BA) were purified by filtration over a basic aluminumoxide column. Potassium peroxodisulfate (99%, KPS) and 4-Styrenesulfonic acid sodium salt hydrate (NaPSS) were purchased from Aldrich and used as received. Ultrapure water, purified by a Millipore system (resistance 18.2 MΩ), was used for emulsion polymerization.

Particle Synthesis. Emulsifier-free emulsion polymerization, adapted from Ottewill,[21] was used for the monodisperse particle synthesis. In a typical recipe, 250 mL of water was heated to 353 K in a thermostat jacketed reaction flask equipped with reflux condenser and an N_2 gas inlet. Total monomer (10 mL, i.e., 9 mL of MMA and 1 mL of *n*BA for the 10% particles and so on), 20 mg NaPSS, and 200 mg KPS were sequentially charged into the reactor. The reaction was carried out overnight for about 16 h under an N_2 inert atmosphere and vigorous stirring with a magnetic stirrer. The dispersions were used without further purification.

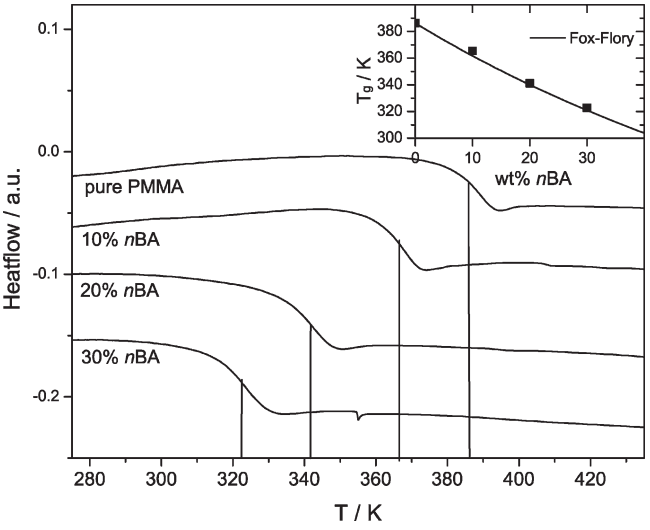

Figure 1. DSC traces for the PMMA-*r*-P*n*BA copolymer samples at the second heating run. The vertical solid lines denote the T_g values for the four samples. The inset shows T_g as a function of the composition together with the representation by eq 1.

Dry Particle Film Preparation. Colloidal crystals of the various particles were fabricated from dilute dispersions (∼1 to 2 wt%) by vertical lifting deposition.[22] In typical, clean glass substrates were immersed in ca. 10 mL of dilute dispersions and withdrawn at a speed of 200−400 nm s^{-1}. Temperature and humidity were kept constant during the deposition at 273 K and 50% RH. Nontransparent films of the colloids with thickness of ∼30−50 μm were obtained. Vertical lifting deposition, as used for sample preparation here, has been shown to lead to fcc colloidal crystal formation, as evidenced, for example, by SEM investigation of the colloid crystals.[23]

Polymer Characterization. The colloidal particles were characterized by scanning electron microscopy (SEM, LEO Gemini 1530, Zeiss) with acceleration voltage from 0.4 to 1.0 kV and InLens detection. Particle diameters were determined by averaging over at least 100 particles, which were measured manually using ImageJ. Particles for differential scanning calorimetry (DSC), wide-angle X-ray scattering (WAXS), gel permeation chromatography (GPC), and density measurements were dried at high vacuum at room temperature. DSC measurements were conducted on a Mettler DSC-823 with a heat rate of 10 K min^{-1} to determine T_g, which is identified as the deflection point of the phase transition in the DSC curve. The results of the second heating cycle, that is, after heating initially to 473 K (and therefore bulk properties), are shown in Figure 1. T_g decreases rapidly with increasing amount of *n*BA. Using the value measured for pure PMMA ($T_g = 386 \pm 3$ K) and the literature value for *n*BA (230 K)[24] allows an excellent representation of T_g as a function of the composition by the Fox−Flory equation[25]

$$\frac{1}{T_g} = \frac{\phi_{\mathrm{PMMA}}}{T_{g,\mathrm{PMMA}}} + \frac{\phi_{\mathrm{P}n\mathrm{BA}}}{T_{g,\mathrm{P}n\mathrm{BA}}} \qquad (1)$$

with no fit parameter, as shown in the inset to Figure 1.

The density, ρ, of the copolymers was determined by a density gradient column using aqueous calcium nitrate solutions.[26] The experimental results conform to a weight-average density, using for the density of the homopolymers $\rho_{\mathrm{P}n\mathrm{BA}} = 1.035$ g cm^{-3} and $\rho_{\mathrm{PMMA}} = 1.195$ g cm^{-3}. The average molecular weight, M_n, and the dimensionless polydispersity index (PDI) of the polymers were measured relative to PMMA standards by GPC. For GPC measurements, solutions of about 1 to 2 mg cm^{-3} in THF with toluene as internal standard were prepared. Crystallinity was excluded based on the WAXS patterns. The measured particle properties are itemized in Table 1.

Table 1. Particle and Material Properties of the Investigated Spheres Obtained by SEM (diameter, d), GPC (M_n, polydispersity (PDI)), DSC (T_g), and Density Gradient Column (ρ)

wt % *n*BA	d/nm	M_n/g mol^{-1}	PDI	T_g/K	ρ/g cm^{-3}
0	232	92 500	4.2	386	1.195
10	214	89 500	4.2	365	1.179
20	200	84 200	3.2	341	1.163
30	204	110 000	3.5	323	1.147

Dielectric Spectroscopy. The sample cell is composed of two electrodes with 20 mm in diameter and the sample with a thickness of 50 μm. The dielectric measurements were performed at different temperatures in the range from 133 to 453 K at atmospheric pressure and for frequencies in the range from 10^{-2} to 10^6 Hz using a Novocontrol high-resolution alpha analyzer. Temperature was controlled by a Novocontrol Quatro Cryosystem, which uses N_2 to heat and cool the sample and has an accuracy of ± 0.1 K. The complex dielectric permittivity $\varepsilon^* = \varepsilon' + i\varepsilon''$, where ε' is the real part and ε'' is the imaginary part, is a function of frequency, $\omega = 2\pi f$, temperature, T, and pressure, P, $\varepsilon^* = \varepsilon^*(\omega,T,P)$. In the analysis of the DS spectra, we have used the empirical equation of Havriliak and Negami (HN).[27]

$$\varepsilon^*(T,P,\omega) = \varepsilon_\infty(T,P) + \sum_j \frac{\Delta\varepsilon_j(T,P)}{[1+(i\omega\tau_{\mathrm{HN}_j}(T,P))^{\alpha_j}]^{\gamma_j}} + \frac{\sigma_0(T,P)}{i\varepsilon_f\omega} \quad (2)$$

Here $\varepsilon_\infty(T,P)$ is the high-frequency permittivity, $\tau_{HN}(T,P)$ is the characteristic relaxation time, $\Delta\varepsilon_j(T,P) = \varepsilon_{0,j}(T,P) - \varepsilon_{\infty,j}(T,P)$ is the relaxation strength of the jth relaxation mode ($j = 1$ for higher and $j = 2$ for lower temperatures), α_j and γ_j (with limits $0 < \alpha, \alpha\gamma \leq 1$) describe, respectively, the symmetrical and asymmetrical broadening of the distribution of relaxation times, σ_0 is the dc conductivity, and ε_f is the permittivity of free space. In the fitting procedure, we have used the ε'' values at every temperature, and in some cases, the ε' data were also used as a consistency check. For $\alpha = \gamma = 1$ the HN equation coincides with an ideal Debye relaxation.

The linear rise of the ε'' at lower frequencies is caused by the conductivity ($\varepsilon'' \approx (\sigma_0/\varepsilon_f)\omega^{-1}$), which has been included in the fitting procedure. From τ_{HN}, the relaxation time at maximum loss, τ_{max}, is obtained analytically for each process following

$$\tau_{\max} = \tau_{\mathrm{HN}}\left[\frac{\sin\frac{\pi\alpha}{2+2\gamma}}{\sin\frac{\pi\alpha\gamma}{2+2\gamma}}\right]^{-1/\alpha} \quad (3)$$

The processes that were covered by the strong conductivity contribution were analyzed using the first derivative method of ε' to derive the ε'' as $\varepsilon_{calc}'' = -\pi/2(\partial\varepsilon'/\partial\ln\omega)$, which provides a conduction-free dielectric loss peak.[28]

Brillouin Light Scattering. For the BLS measurements, a Sandercock six-pass tandem Fabry−Pérot interferometer with adjustable free spectral range (fsr used here: 7.5 GHz), actively stabilized by a reference beam, was utilized. A $\lambda = 532$ nm Nd/YAG laser (50 mW) is mounted on a goniometer, allowing for measurements in transmission and reflection geometry at scattering angles $3 \leq \theta \leq 150°$ (cf. Figure 1 in ref 12). The particle eigenmode BLS spectra were recorded in transmission geometry at (nonarbitrative, due to strong multiple scattering) scattering angle of 50°.[11] To obtain the longitudinal sound velocity in the bulk materials for reliable input to the theoretical description of the particle vibration eigenfrequencies, **q**-dependent BLS spectra of transparent films were recorded. These films (with thickness $\approx 3-5$ m) have been prepared by melting the opals by a heat gun ($T \approx 400-450$ K) for a few seconds. Figure 2 shows

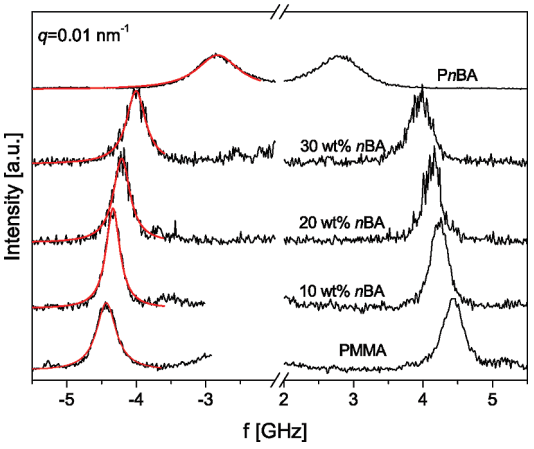

Figure 2. Exemplary polarized BLS spectra of bulk PMMA, P*n*BA, and PMMA-*r*-P*n*BA copolymers at $q = 0.01$ nm^{-1} and room temperature. The red lines on the Stokes side of the spectra are single Lorentzian fits of the signals.

polarized BLS spectra of bulk PMMA, P*n*BA, and the three PMMA-*r*-P*n*BA copolymers at room temperature (395 K) for an exemplary $q = 0.01$ nm^{-1}. The single doublet characteristic of a homogeneous film on length scales shorter then q^{-1} peaks at the Brillouin shift, ω_B, which for a purely acoustic excitation yields the frequency-independent phase sound velocity $c_l = \omega_B/q$. The value of c_l decreases from 2755 m s^{-1} in PMMA to 1835 m s^{-1} in P*n*BA. Equivalently, M drops from 9.1 to 3.5 GPa, also taking into account the ~15% lower density of P*n*BA. These values indicate a reasonably high mechanical contrast between the two components and hence hold promise for an adequate variation of $M(\phi)$. Owing to the very low anisotropic scattering of these polymers and relatively thin films, depolarized BLS spectra are hardly discernible, which would preclude access to c_t and G.

Data Analysis and Results

Copolymerization of two distinct monomers permits the combination of their individual properties and hence allows control over various physical quantities. Random radical emulsion copolymerization of MMA and *n*BA was conducted to tune the thermomechanical properties of the resulting colloidal particles. The composition of *n*BA in the copolymer was targeted to 10, 20, and 30 wt % by adjusting the weight ratio of the two monomers in the initial emulsion. On the basis of the given density data, this corresponds to $\phi(n\mathrm{BA}) = 0.088$, 0.178, and 0.271, respectively. A random copolymerization is indicated by the Q and e values of both monomers in terms of the Q-e-schema of Alfrey and Price (*n*BA: $Q = 0.38$, $e = 0.85$; MMA: $Q = 0.78$, $e = 0.40$).[29,30] A homogeneous copolymerization is indicated by the very similar r values (*n*BA: $r = 0.94$; MMA: $r = 0.91$) not very different from $r = 1$.

The three statistical copolymers PMMA-*r*-P*n*BA display a single T_g (Figure 1) despite the fact that the two homopolymers possess very high T_g contrast ($T_{g,PMMA} \approx 383$ K, $T_{gPnBA} \approx 230$ K). For the copolymer with 30 wt % *n*BA, T_g drops 63 K below $T_{g,PMMA}$. The presence of a single T_g, however, is a necessary but not sufficient condition for complete miscibility on short length scales. Only the nature of the segmental dynamics can unambigously decide local miscibility. The large T_g contrast ($T_{g,PMMA}/T_{g,PnBA} - 1 \approx 0.7$) implies very different free volume, which, in turn, justifies similarly large elastic impedance contrast $\Delta Z/\Delta Z = \rho_{PMMA}c_{PMMA}/\rho_{PnBA}c_{PnBA} - 1 \approx 0.5$ between the two homopolymers. Hence, the expected variation of the elastic properties of the copolymer particles with composition should impact their vibration eigenfrequencies.

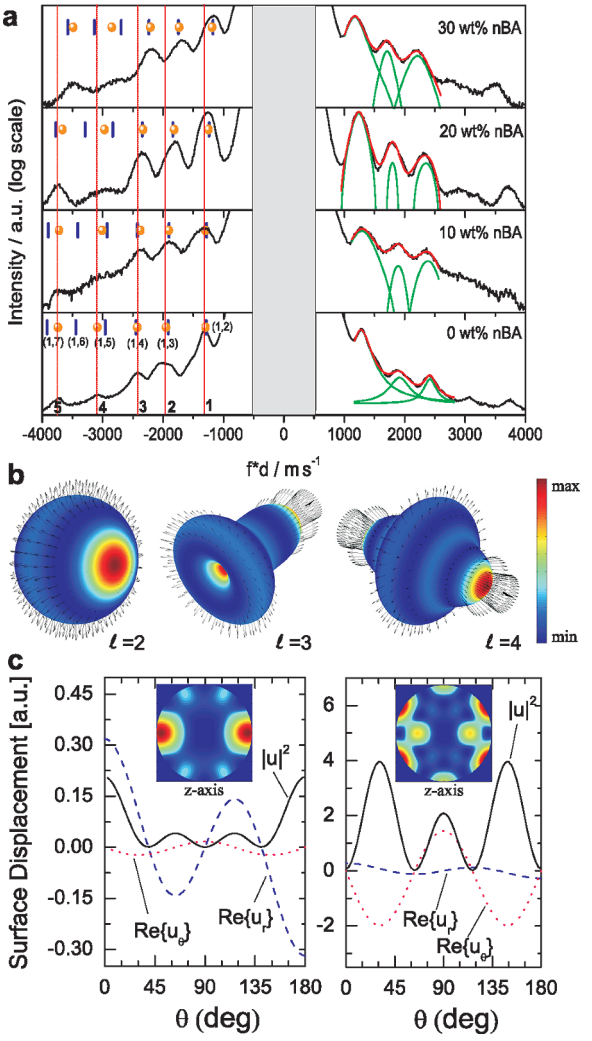

Figure 3. (a) Experimental BLS eigenmode spectra versus a reduced frequency, fd, with d being the particle diameter. The dotted red vertical lines on the Stokes side denote the positions of the five resolved maxima for the pure PMMA spheres. The orange dots and the short blue vertical lines denote, respectively, the experimental and the computed resonance frequencies (n,l) for the four particles. (b) Shape of the first three eigenmodes with $n = 1$ for a pure PMMA sphere in air through single-sphere scattering calculations, verified also by FEM simulations for the corresponding free vibrating sphere. Deformation is enlarged by an appropriate factor for a better visualization; the color scale shows total displacement. The axis of incidence, z, is the axis of rotational symmetry. (c) (1,3) L- and P-mode (left and right plots) for the pure PMMA particle. The total intensity, $|u|^2$, and the real parts of the radial, u_r, and tangential, u_θ, components of the displacement field on the circumference of the sphere are shown (solid, dashed, and dotted curves, respectively) together with a 2D plot cut of the sphere passing on its center; the axis of incidence of the external acoustic plane wave directed from left to right, is taken as z axis (i.e., $\theta = 0$).

Particle Vibrational Frequencies. Films of fcc-arranged mesoscopic polymer spheres in air behave as an ensemble of independent particles, sustaining vibrational modes due to the thermal energy.[10−12] Figure 3a shows the BLS eigenmode spectra for the four opals. Because the eigenfrequencies of colloidal particles scale with d^{-1},[31] the spectra are plotted versus fd. The resonance peaks can therefore be identified by direct comparison to the single sphere's modes. These resonance modes can be theoretically obtained through rigorously exact single-sphere scattering-matrix calculations combined with DOS techniques,[32,33] but their frequencies can be approximately described by the eigensolutions of a free-vibrating solid sphere[31] with sphere diameter, d

Table 2. Experimental, c_l, Fitted, c_t, elastic Moduli (Young's, Longitudinal, and Shear Modulus), and Poisson's Ratio[a]

wt % *n*BA	c_l	c_t/ms^{-1}	E/GPa	M/GPa	G/GPa	σ
0	2755	1530	7.14	9.07	2.80	0.277
10	2678	1520	6.88	8.46	2.72	0.262
20	2615	1466	6.35	7.95	2.50	0.271
30	2498	1394	5.68	7.15	2.23	0.274

[a] For a maximum error of ±2% for c_l and c_t, the maximum relative errors are approximately 5% for σ and 4% for E, M, and G.

$$f(n,l,\sigma) = \frac{c_t}{d} a(n,l,\sigma) \quad (4)$$

where $a(n,l,\sigma)$ is a constant for each individual spheroidal resonance mode (n,l), that is, the nth order mode of the lth spherical harmonic and with Poisson's ratio $\sigma = (c_l^2 - 2c_t^2)/2(c_l^2 - c_t^2)$. According to eq 4, decrease in the shear modulus G, that is, softening, with increasing *n*BA content leads to a red shift of the eigenmodes. The vertical lines on the Stokes side of Figure 3a help to visualize this frequency shift. Notably, the decrease in the density with increasing *n*BA content alone, that is, for an unchanged G, would lead to a frequency shift in the opposite direction. All four spectra can be represented by five Lorentzian lineshapes, as indicated for the strongest first three eigenmodes by the green solid lines on the anti-Stokes side of the spectra of Figure 3a. The peak positions of the Lorentzian lines are indicated by the orange dots on the Stokes side of the spectra; the fourth spectral line around $fd \approx 3000$ m s^{-1} is broader and less pronounced than the others.

According to eq 4, the frequency of the eigenmodes is a function of c_t and σ or, alternatively, G, σ, and ρ since G is a function of ρ and c_t. Because the mass density is experimentally known, the remaining adjustable parameters are G and σ, or c_t and c_l, respectively. On the basis of earlier studies of the vibration eigenmodes of colloidal particles, the value of c_l does not deviate from the corresponding value in the bulk material,[11,12,34] for which c_l is easily accessible by q-dependent BLS.

Theoretically, the frequencies of the spheroidal eigenmodes $f(n,l)$ depend strongly on c_t but are rather insensitive to the variation of c_l, as concluded by DOS and finite element (FEM) calculations for $n = 1$. This justifies the use of c_l measured for bulk systems as a fixed parameter. (See Table 2.) Therefore, the DOS calculations for a polymer sphere in air were performed focusing first in the three strongest lower frequency modes, using only one floating parameter (c_t).[33] Utilizing reasonable values for c_t, the first three modes could be clearly assigned to the (1,2), (1,3), and (1,4) L modes of a solid sphere by analogy to the results found in polystyrene latex particles.[11] The 3D representation of these eigenmodes is shown in Figure 3b. We denote as L modes the solutions of the sphere, classified as spheroidal modes for a free vibrating sphere, which are characterized by almost radial displacement at the surface of the sphere (the radial component, u_r, dominates the tangential one, u_θ) and they have maximum surface displacement value along the axis of incidence, z ($\theta = 0,\pi$), of the acoustic plane wave incident on the sphere. (See Figure 3c.) The purely radial $l = 0$ mode, known also as breathing mode, belongs to the same family. Its frequency, for a polymer sphere in air, is systematically located before and close to the $l = 4$ mode ($fd \approx 2298$, 2207, 2170, and 2078 m s^{-1}, respectively, for the

four specimens of Figure 3a from bottom to top) and therefore cannot be resolved.

Modes directed mostly along polar (θ-) direction, tangentially to the sphere surface, appear at higher frequencies (these (1,1), (1,2), (1,3), and (1,4) modes are calculated at $fd \approx$ 1696, 2407, 3184, and 3964 m s^{-1}, respectively, for the case of the pure PMMA sphere). Contrary to L modes, their surface displacement is minimum on the axis of incidence, z, that is, for $\theta = 0,\pi$. (See right plot of Figure 3c.) They do not manifest themselves as strong peaks in the BLS spectra, probably buried in the background. We denote them as P modes and further ignore them in the fitting procedure. We note here that P modes do not have to be confused with the torsional modes of a sphere, purely shear, creating a rotatory mouvement along the azimuthal (ϕ-) direction. These modes cannot be excited by a longitudinal acoustic wave incident on the sphere and remain inactive during the BLS excitation process.[16]

In fact, there have been discussions on the assignment of the L-type eigenmodes. According to Kuok and coworkers,[35] there should be selection rules in BLS allowing only the detection of even l modes (similar to Raman scattering[17]). However, because of retardation effects when the particle diameter becomes similar to the wavelength of the scattered light, modes with odd l become also accessible,[16] which is in good agreement with experimental results, for example, the representation of 21 eigenmodes in polystyrene spheres with no adjustable parameter[11] and FEM modeling of free vibrating spheres.[12]

Apart from the first three strong peaks that guide the fitting process, the fourth BLS signal is much broader than the others in all four samples and cannot be assigned to the expected (1,5) L mode, which occurs at lower frequencies. Indeed, the fourth mode's frequency falls between the (1,5) and (1,6) L modes, suggesting the superposition of both modes, which accounts for the broad appearance of the fourth peak. The "fifth" mode can be assigned to the computed (1,7) L mode using the value of c_t as obtained from the representation of the three lower frequency modes in the BLS spectra. For the "fifth" mode, the disparity between experiment and theory decreases with increasing amount of *n*BA in the copolymer. In this context, it should be noted that the (2,1) P mode lies in the vicinity of (1,7) L mode for the utilized set of c_t and c_l values. In this frequency range, the assignment of this experimental vibration to either of the two theoretical modes seems to be ambiguous.

The frequencies of the experimentally observed particle vibrations in the four particles are shown in Figure 4 along with the theoretically predicted values fd using c_t as the single adjustable parameter. From these c_t values and the measured c_l and ρ the elastic moduli and the Poisson's ratio of the copolymer PMMA-*r*P*n*BA mesospheres are computed, which quantify their softening with *n*BA composition. Table 2 is a compilation of the two sound velocities, the different moduli, and the Poisson's ratio of the statistical-copolymer-based colloidal particles. The monotonic variation of the sound velocities with *n*BA composition along with the single T_g should be reflected in the modality of the segmental dynamics in these systems.

Segmental Dynamics. The presence of the single T_g found in DSC is not a sufficient condition for local segmental miscibility because the system can still display two distinct primary α-relaxation processes.[36−38] Because both MMA and *n*BA repeat units possess a permanent dipole moment normal to the chain backbone, DS is the appropriate technique to address the local polymer dynamics. Figure 5a shows representative spectra of the real (top) and the imaginary

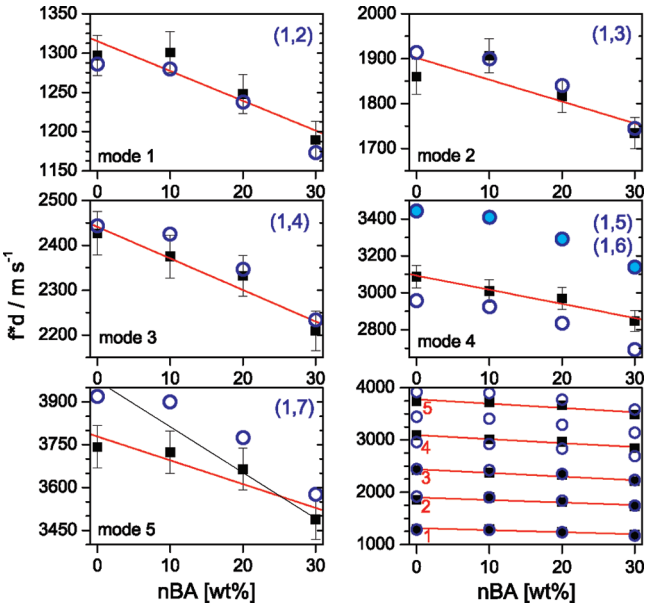

Figure 4. Reduced frequency, fd, (■) for all experimentally observed vibrations (modes 1−5) as a function of the *n*BA composition in each of the four colloidal particles. The empty circles indicate the computed (see text) frequencies for the particle eigenmodes (1,l) with l = 2−7 (● for (1,6)-mode). The red lines are guides for the eyes, and the error bars amounts to 2%. For comparison, the bottom right panel shows the dependence of fd on *n*BA composition for all five modes.

(bottom) part of the complex dielectric function for the 20 wt % *n*BA sample at temperatures in the range of 333 to 393 K in steps of 10 K. The ε^* spectra were represented by eq 2. The increase in temperature combines the α- (with HN shape parameters: $\alpha = 0.4 \pm 0.05$, $\alpha\gamma = 0.15$) and β-processes (HN shape parameters: $\alpha = 0.38 \pm 0.05$, $\alpha\gamma = 0.18$) into a single ($\alpha\beta$)-process (HN shape parameters: $\alpha = 0.6 \pm 0.03$, $\alpha\gamma = 0.62$). There have been many publications concerning the multiple relaxations and the merging/coalescence behavior in poly(*n*-alkylmethacrylates),[39] but this is not of main interest in the present investigation. $\varepsilon''(\omega)$ at 363 K for PMMA and the three copolymers are compared in Figure 5b. It is clear, that the increase in the *n*BA content accelerates the dielectric processes. The same is more obvious in Figure 5c, where the temperature dependence of the relaxation times at maximum loss (eq 3) for the three processes is presented. The β-process (local motion) shown in the low-temperature regime displays an Arrhenius temperature dependence with activation energy E (for PMMA: $E = 85.3$ kJ mol^{-1} and for the copolymers $E = 77 \pm 2$ kJ mol^{-1}). At higher temperatures, the α- (associated with glass transition) and $\alpha\beta$-processes display a much stronger temperature dependence than the β-process. These processes can be described using the Vogel−Fulcher−Tammann (VFT) equation. (See ref 40 for details.)[41] In addition to the single T_g, DS shows a single α-relaxation for each sample; that is, both kinds of monomer segments feel the same local environment.[36−38]

Discussion and Conclusions

So far, the main result of the article is the measurement of the elastic constants of mesoscopic colloidal particles and their facile tuning by means of a random copolymerization of two monomers, whose corresponding homopolymers possess large T_g contrast. Table 3 shows the decrease in c_l with increasing amount of *n*BA. However, this decrease is relatively small compared with the large T_g contrast and the difference between the values of c_l in the two homopolymers. Several approaches to describe the sound

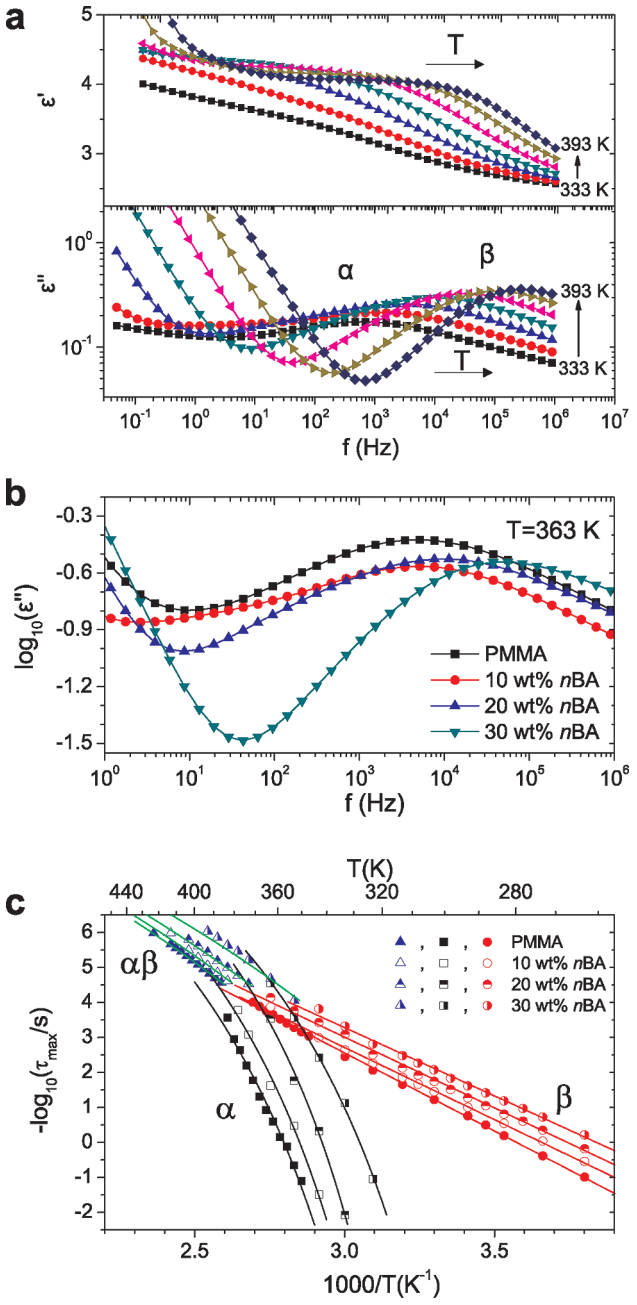

Figure 5. (a) Real (top) and imaginary (bottom) part of the complex dielectric permittivity as a function of frequency for the 20 wt % *n*BA sample at different temperatures. Each curve corresponds to different temperatures between 333 and 393 K in steps of 10 K. α and β indicate the primary segmental (related to the glass transition) and secondary process, respectively. (b) Dielectric loss curves for the materials investigated herein as a function of frequency at 363 K. (c) Temperature dependence of the relaxation times at maximum loss for the three resolved processes: The ($\alpha\beta$)-process (▲) and the α- (■) and the β- (●) processes. The lines denote fits of the VFT equation for the ($\alpha\beta$)- and α-processes and the Arrhenius equation for the β-process.

propagation in an effective medium composed of (at least) two mechanically different materials have been discussed.[42,43] It turns out that the simple expression

$$\frac{1}{M_{\mathrm{eff}}} = \frac{\phi_1}{M_1} + \frac{1-\phi_1}{M_2} \qquad (5)$$

which is known as Wood's law,[7] is in many cases a good representation of the effective modulus M_{eff} as a function of the bulk component moduli (M_1, M_2) and their proportions by volume (ϕ_1, $1 - \phi_1$). If one assumes Wood's law to be, in principle, a good approximation also for copolymers, the theoretically expected values for c_l can be easily calculated, as shown in the third column of Table 3. Obviously, the presented approximation strongly overestimates the softening with increasing *n*BA fraction, leading to a deviation of up to 7% for c_l in the 30 wt % *n*BA sample or ~14% for M compared with the experimental value given in Table 2. A possible source of the deviation can be the validity of the value M_1 for the bulk P*n*BA because this is the only polymer among the other four systems that is in the rubbery and not in the glassy state at 395 K.

Table 3. Experimental and Theoretical Bulk c_l (in m s^{-1}) for Homopolymers and Copolymers at Room Temperature[a]

wt % *n*BA	c_l (BLS)	c_l (Wood) exp. $c_{l,PnBA}$	dev (%)	c_l (Wood) $c_{l,PnBA}$ = **2154** m s^{-1}	dev (%)
0	2755	2755		2755	
10	2678	2594	−3.2	2669	−0.3
20	2615	2460	−6.3	2591	−0.9
30	2498	2343	−6.7	2519	+0.8
100	*1835*	*1835*		**2154**	

[a] Theoretical values for the copolymers are calculated using eq 5 with experimental or fictive "glassy" $c_{l,PnBA}$, respectively. The relative deviation to the experimental c_l is given for both columns.

The mechanical moduli are temperature- and frequency-dependent. At room temperature and GHz frequencies, the sound velocities for all examined bulk polymers but P*n*BA correspond to the glassy state, and these polymers are, therefore, fully elastic solids. In contrast, bulk P*n*BA at room temperature exist in the rubbery (viscoelastic) regime. Therefore, c_l is lower than it would be for a glassy P*n*BA at the same temperature. This is apparent from the broader BLS spectrum of P*n*BA compared with the other polymers in Figure 2 due to phonon dissipation. For nanoscopically completely homogeneous copolymers, M_1 must assume a higher value than in bulk P*n*BA because the *n*BA segments in the three glassy PMMA-r-P*n*BA copolymers sense denser packing of the glassy and not the higher free volume of the rubber state above T_g. The conjecture of an ideal miscibility is strongly supported by the segmental dynamics. The presence of a single α-relaxation in the DS experiments for all PMMA-*r*-P*n*BA copolymers indicates homogeneous segmental dynamics, which in turn implies a local effective medium behavior, that is, on the length scale of the Kuhn segment. This is, in its own, an unexpected result, considering the large T_g contrast of the two homopolymers, which usually boosts dynamic heterogeneities.[2,36−38] Because at ambient temperature the three copolymers and PMMA are in the glassy state, the *n*BA segments are also dynamically frozen. Therefore, the substitution of M_1 by the bulk P*n*BA value in the rubbery state (above T_g) must be erroneous.

The success of eq 5 in representing the experimental c_l values of the copolymers is optimized if $c_{l,PnBA}$ = 2154 m s^{-1} is used for the bulk P*n*BA in its fictive glassy state at 395 K. Indeed, this value is ~17% higher than the experimental $c_{l,PnBA}$ (1835 m s^{-1}) of the bulk P*n*BA in the rubbery state at the same temperature. The fifth column in Table 3 demonstrates the improved agreement between experiment and eq 5, using this artificially increased value.

It is worth to mention, however, the unexpected robustness of σ over the examined composition range with a concurrent T_g drop of 63 K between pure PMMA and the 30 wt % *n*BA sample. Because all copolymers are still in the glassy state at room temperature, this finding suggests a very similar temperature dependence of the two sound velocities in the present systems.

In summary, this work presents a systematic study of the thermomechanical properties of mesoscopic colloidal particles formed by a random copolymerization of MMA and *n*BA

monomers. BLS, WAXS, and DS experiments revealed an amorphous morphology and complete miscibility at the monomer level, which is supported by the dynamic homogeneity of this copolymer system, despite the large T_g contrast of the constituent components. BLS of the copolymer latex particles recorded the spectrum of spheroidal vibration eigenmodes, which sensitively depend on the shear modulus of these mesoscopic spheres, as shown by detailed DOS calculations. This is important in metrology because c_t can be hardly measured for the same weakly anisotropic polymers (very weak depolarized scattering) in contrast with the readily accessible c_l from the polarized BLS spectra of bulk polymers.

The DOS calculations support a virtually constant Poisson's ratio $\sigma \approx 0.27$ in all glassy copolymer particles. The longitudinal moduli are well-represented by the effective medium Wood's law (eq 5) assuming, however, a 38% higher longitudinal modulus than the measured value in the bulk P*n*BA. This apparently peculiar assumption is in full agreement with the dynamic homogeneity of these copolymer particles. Bulk P*n*BA is in the rubbery state at ambient temperature in contrast with the glassy copolymer particles. The random copolymerization of MMA and *n*BA leads to a fully miscible system with tunable mechanical properties while exhibiting homogeneous segmental dynamics despite the high T_g contrast of the constituent homopolymers.

Acknowledgment. We want to thank P. Räder for DSC, S. Seywald for GPC, M. Bach for WAXS, and G. Schäfer for density measurements as well as K.-H. Dostert for help with particle synthesis. M.R. thanks the VCI for the Kekulé scholarship. G.F. acknowledges partial support by DFG (Grant-JO-370/2-1).

References and Notes

(1) Maranas, J. K. *Curr. Opin. Colloid Interface Sci.* **2007**, *12*, 29.
(2) Leroy, E.; Alegria, A.; Colmenero, J. *Macromolecules* **2003**, *36*, 7280.
(3) Mpoukouvalas, K.; Floudas, G. *Macromolecules* **2008**, *41*, 1552.
(4) Rizos, A. K.; Fytas, G.; Roovers, J. E. L. *J. Chem. Phys.* **1992**, *97*, 6925.
(5) Kanetakis, J.; Fytas, G.; Kremer, F.; Pakula, T. *Macromolecules* **1992**, *25*, 3484.
(6) Mpoukouvalas, K.; Floudas, G.; Verdonck, B.; Du Prez, F. E. *Phys. Rev. E* **2005**, *72*, 011802.
(7) Wood, A. B. *Textbook of Sound*; Macmillan: New York, 1941.
(8) Mei, J.; Liu, Z.; Wen, W.; Sheng, P. *Phys. Rev. Lett.* **2006**, *96*, 024301.
(9) Takagi, S.; Tanaka, H. *Phys. Rev. E* **2010**, *81*, 021401.
(10) Kuok, M. H.; Lim, H. S.; Ng, S. C.; Liu, N. N.; Wang, Z. K. *Phys. Rev. Lett.* **2003**, *90*, 255502.
(11) Cheng, W.; Wang, J. J.; Jonas, U.; Steffen, W.; Fytas, G.; Penciu, R. S.; Economou, E. N. *J. Chem. Phys.* **2005**, *123*, 121104.
(12) Still, T.; Cheng, W.; Retsch, M.; Jonas, U.; Fytas, G. *J. Phys.: Condens. Matter* **2008**, *20*, 404203.
(13) Still, T.; Sainidou, R.; Retsch, M.; Jonas, U.; Spahn, P.; Hellmann, G. P.; Fytas, G. *Nano Lett.* **2008**, *8*, 3194.
(14) Still, T.; D'Acunzi, M.; Vollmer, D.; Fytas, G. *J. Colloid Interface Sci.* **2009**, *340*, 42.
(15) Duval, E.; Boukenter, A.; Champagnon, B. *Phys. Rev. Lett.* **1986**, *56*, 2052.
(16) Montagna, M. *Phys. Rev. B* **2008**, *77*, 045418.
(17) Duval, E. n. *Phys. Rev. B* **1992**, *46*, 5795.
(18) Montagna, M.; Dusi, R. *Phys. Rev. B* **1995**, *52*, 10080.
(19) Akimov, A. V.; Tanaka, Y.; Pevtsov, A. B.; Kaplan, S. F.; Golubev, V. G.; Tamura, S.; Yakovlev, D. R.; Bayer, M. *Phys. Rev. Lett.* **2008**, *101*, 033902.
(20) Pelton, M.; Sader, J. E.; Burgin, J.; Liu, M.; Guyot-Sionnest, P.; Gosztola, D. *Nat. Nanotechnol.* **2009**, *4*, 492.
(21) Goodwin, J. W.; Hearn, J.; Ho, C. C.; Ottewill, R. H. *Colloid Polym. Sci.* **1974**, *252*, 464.
(22) Dimitrov, A. S.; Nagayama, K. *Langmuir* **1996**, *12*, 1303.
(23) Jiang, P.; Bertone, J. F.; Hwang, K. S.; Colvin, V. L. *Chem. Mater.* **1999**, *11*, 2132.
(24) Penzel, E.; Rieger, J.; Schneider, H. A. *Polymer* **1997**, *38*, 325.
(25) Strobl, G. *The Physics of Polymers*, 2nd ed.; Springer: Berlin, 1997.
(26) Linderstrom-Lang, K. *Nature* **1937**, *139*, 713.
(27) Havriliak, S.; Negami, S. *Polymer* **1967**, *8*, 161.
(28) Wübbenhorst, M.; Koten, E. M. V.; Jansen, J. C.; Mijs, W.; Turnhout, J. v. *Macromol. Rapid Commun.* **1997**, *18*, 139.
(29) Alfrey, T.; Price, C. C. *J. Polym. Sci.* **1947**, *2*, 101.
(30) Greenley, R. Z. *Polymer Handbook*, 4th ed.; Wiley: Hoboken, NJ, 1999; Vol. *1*.
(31) Lamb, H. *Proc. London Math. Soc.* **1882**, *s1−13*, 189.
(32) Flax, L.; Dragonette, L. R.; Uberall, H. *J. Acoust. Soc. Am.* **1978**, *63*, 723.
(33) Sainidou, R.; Stefanou, N.; Modinos, A. *Phys. Rev. B* **2004**, *69*, 064301.
(34) Lim, H. S.; Kuok, M. H.; Ng, S. C.; Wang, Z. K. *Appl. Phys. Lett.* **2004**, *84*, 4182.
(35) Li, Y.; Lim, H. S.; Ng, S. C.; Wang, Z. K.; Kuok, M. H. *Chem. Phys. Lett.* **2008**, *461*, 111.
(36) Kumar, S. K.; Colby, R. H.; Anastasiadis, S. H.; Fytas, G. *J. Chem. Phys.* **1996**, *105*, 3777.
(37) He, Y.; Lutz, T. R.; Ediger, M. D. *J. Chem. Phys.* **2003**, *119*, 9956.
(38) Lodge, T. P.; McLeish, T. C. B. *Macromolecules* **2000**, *33*, 5278.
(39) Mpoukouvalas, K.; Floudas, G.; Williams, G. *Macromolecules* **2009**, *42*, 4690.
(40) $\tau_{max} = \tau_0 \exp(D_T T_0/(T - T_0))$; τ_0 is the relaxation time in the limit of high temperatures, D_T is a dimensionless parameter related to the activation energy, and T_0 is the Vogel temperature. In the present study, the following VFT parameters have been used: for the α-process in PMMA, $\tau_0 \approx 10^{-14}$ s, $D_T = 10.5 \pm 0.2$, and $T_0 = 270 \pm 1$ K and for the copolymers $\tau_0 \approx 10^{-14}$ s, $D_T = 9 \pm 0.5$, and $T_0 = 270-255$ K. For the αβ-process, in PMMA $\tau_0 \approx 10^{-14}$ s, $D_T = 27 \pm 0.1$, and $T_0 = 171 \pm 1$ K and for the copolymers $\tau_0 \approx 10^{-14}$ s, $D_T = 27 \pm 0.1$, and $T_0 = 170-160$ K.
(41) Ferry, J. D. *Viscoelastic Properties of Polymers*, 3rd ed.; Wiley: New York, 1980.
(42) Gaunaurd, G. C.; Wertman, W. *J. Acoust. Soc. Am.* **1989**, *85*, 541.
(43) Waterman, P. C.; Truell, R. J. *Math. Phys.* **1961**, *2*, 512.